Journal of
Applied Crystallography

ISSN 0021-8898

Received 22 December 2011
Accepted 17 April 2012

Unidirectional crystal growth and crystalline perfection of L-arginine phosphate monohydrate

B. Riscob,[a,b] Mohd Shakir,[a] N. Vijayan,[a] K. K. Maurya,[a] M. A. Wahab[b] and G. Bhagavannarayana[a]*

[a]National Physical Laboratory, Council of Scientific and Industrial Research, Dr K. S. Krishnan Road, New Delhi, 110 012, India, and [b]Department of Physics, Jamia Millia Islamia, New Delhi, 110 025, India. Correspondence e-mail: bhagavan@mail.nplindia.ernet.in

A large (~20 mm diameter and 80 mm length) single crystal of L-arginine phosphate monohydrate (LAP) has been grown for the first time by the unidirectional Sankaranarayanan–Ramasamy method in an aqueous medium in a specially designed constant-temperature bath. The crystal structure has been confirmed by powder X-ray diffraction. The crystalline perfection was assessed by high-resolution X-ray diffractometry (HRXRD) which found that the quality of the grown single crystal is quite good. HRXRD studies along different directions show that the crystal contains a low density of edge-type dislocations formed along the growth direction. The thermal stability was assessed using thermogravimetric/differential thermal analysis. The mechanical behaviour was studied using an Omnitech micro-hardness tester. The dielectric studies were carried out over a wide frequency range of 10 Hz to 5 MHz at room temperature. The characterization studies reveal that the grown bulk single crystal of LAP is suitable for device applications.

1. Introduction

The technological world depends upon the growth of high-quality defect-free bulk-size single crystals for device fabrication in various fields of application. Selection of the growth technique is very important in growing bulk-size single crystals. The slow evaporation solution technique is an established method for growing single crystals from solution, but it is not suitable for growing a bulk crystal because of the growth of various facets along different directions, including unwanted multi-nucleation, over which there is little control. By using the recently invented unidirectional Sankaranarayanan–Ramasamy (SR) method (Sankaranarayanan & Ramasamy, 2005), which retains the basic principles of the slow evaporation solution method, it is possible to grow bulk-size crystals along the desired direction with a simple apparatus. This method also has the advantage of nearly 100% solute–crystal conversion efficiency.

Nonlinear optical (NLO) materials play a key role in the area of photonics for optical information storage, processing (Misoguti *et al.*, 1996) and communication *etc*. They are also important for high-energy lasers for inertial confinement fusion research (Zaitseva & Carman, 2001), colour displays, electro-optic switches, frequency conversion *etc*. (Badan *et al.*, 1993). For device applications, it is essential that crystals are a good size along the desired direction and have good crystalline perfection. The SR method is an appropriate technique for growing bulk crystals of materials such as potassium dihydrogen phosphate (KDP), bis(thiourea)zinc(II) chloride, potassium ammonium phosphate and L-cysteine hydrochloride monohydrate (Balamurugan & Ramasamy, 2009; Kushwaha *et al.*, 2008; Senthil Pandian *et al.*, 2008; Bhagavannarayana, Kumar *et al.*, 2010). In any solution growth method, either in the conventional slow evaporation or in the SR method, the concentration at the solid–liquid interface cannot be identical throughout the growth process, though it is theoretically possible with well estimated controlled evaporation. This is also true in the case of the temperature-lowering solution growth method and causes the formation of point defects, their clusters and dislocations. When the density of such defects is very high in single crystals, structural grain boundaries and a variety of bulk defects such as entrapment of solvent (Bhagavannarayana, Rajesh & Ramasamy, 2010) may occur. High-resolution X-ray diffractometry (HRXRD) is a powerful technique for revealing most of these defects in a nondestructive way (Senthil Kumar *et al.*, 2011).

L-Arginine phosphate monohydrate (LAP), an excellent NLO material, crystallizes in the monoclinic space group $P2_1$ as reported by Monaco *et al.* (1987). Electron paramagnetic resonance and optical absorption studies of VO^{2+} ions in LAP have been conducted at room temperature (Mary & Dhanuskodi, 2001). Rare-earth-doped and amino acid-doped LAP crystals have been systematically studied for their structural and optical properties and their thermal behaviour (Arjunan *et al.*, 2010; Anandan *et al.*, 2011). An atomic force microscopy study of the (100) cleaved plane of an LAP crystal has been carried out (Sangwal, Servat *et al.*, 1997; Sangwal, Torrent-Burgues *et al.*, 1997). Optically finished surfaces have been prepared by diamond turning (Baruch *et al.*, 1989).

Temperature-dependent optical anisotropy (Herreros-Cedres *et al.*, 2003) and second harmonic generation (SHG) have also been studied; the latter was found to be three times that of KDP (Hameed & Rohani, 2007). Along with the search for new, suitable NLO materials, it is equally important to assess the perfection of the grown crystals from the device fabrication point of view. Many of the properties are direction dependent and can be masked or significantly diminished when they are not in the single-crystal domain or the crystals have defects such as structural grain boundaries (Bhagavannarayana, Ananthamurthy *et al.*, 2005; Bhagavannarayana, Budakoti *et al.*, 2005). It is therefore very important to assess the crystalline perfection of the grown crystals, including the possible crystallographic direction dependency of physical properties, to ascertain their suitability for device application/fabrication.

In the present investigation, good-quality bulk single crystals of LAP were grown by the SR method for the first time in an aqueous medium. The structure was confirmed by the single-crystal X-ray diffraction (XRD) technique. Crystalline perfection was assessed by HRXRD along different crystallographic directions. We also investigated the mechanical strength and dielectic properties. Though we have not described the details, the functional groups of the title compound were studied and confirmed by FT–Raman analysis as reported by Dhanaraj *et al.* (1991); the optical transparency was checked by UV–visible spectroscopic analysis and is in agreement with that reported by Anandan *et al.* (2011). SHG analysis was also carried out and confirmed, with a reported SHG efficiency of three times that of the standard KDP (Baruch *et al.*, 1989).

2. Experimental

2.1. Crystal growth

To grow the LAP single crystal by the SR method, a defect-free small seed crystal is necessary. The seed crystal was grown by the slow evaporation solution technique by taking an equimolar ratio of L-arginine and orthophosphoric acid. This product was synthesized in deionized water by the procedure reported earlier (Monaco *et al.*, 1987). The purity of the synthesized salt was enriched by repeated recrystallization processes. A saturated solution of the synthesized salt was prepared by using the solubility curve (Hameed & Rohani, 2007; Kim & Lal, 1998). The saturated solution was prepared at room temperature with continuous stirring for 24 h and kept undisturbed in a beaker covered with a polythene sheet in which there were fine holes. Good-quality transparent single crystals were harvested from the mother solution after a period of 25 d. A well faceted as-grown crystal was prepared carefully along the [010] direction and used as a seed crystal for SR growth.

The SR ampoule, made of ordinary glass, is described in our earlier article (Kushwaha *et al.*, 2008). It has a tapered 'V'-shaped bottom (where the seed crystal is mounted vertically along [010]) and a 'U'-shaped larger-diameter top portion which may be filled with a good amount of supersaturated solution to grow a bulk-size crystal. The cylindrical portion connects the tapered 'V'-shaped bottom and 'U'-shaped top portions. The ampoule was cleaned well with acetone and dried in an oven. The prepared saturated solution was poured into the SR ampoule without disturbing the seed crystal. The top portion of the tube was covered with a fine plastic sheet to avoid fast evaporation and a few holes were made in the sheet to start growth by slow evaporation. The SR ampoule was housed in a specially designed constant-temperature bath to control spurious nucleation as well as the growth rate of the crystal. The growth rate is important from the viewpoint of a single crystal's performance in device applications (see below). The experimental conditions were closely monitored to determine the growth of the seed crystal and it was observed that after a period of 18 d the size of the seed crystal had started to increase. The size of the crystal improved well with time and the growth rate was adjusted by varying the temperature using a temperature controller, reducing it to obtain a well ordered defect-free transparent single crystal. After 80 d a good-quality highly transparent 80 mm-long single crystal of LAP was harvested. Figs. 1(*a*) and 1(*b*) show the crystal when it is inside and outside the SR ampoule, respectively. The crystal has a few good facets which are indexed with Miller indices as shown in Fig. 1(*c*). It may be

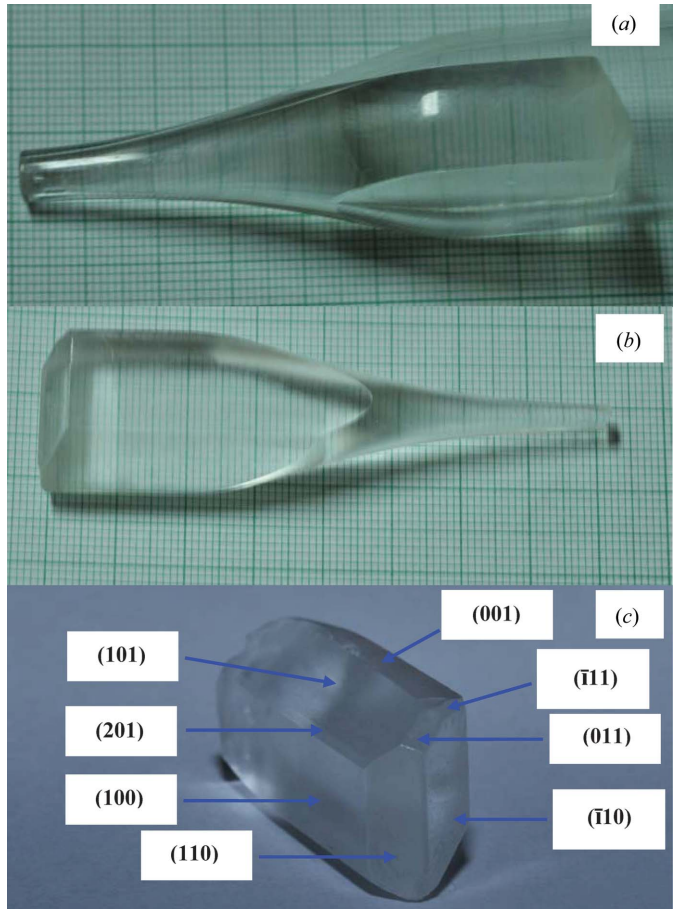

Figure 1
LAP single crystal: (*a*) inside and (*b*) outside the SR ampoule, and (*c*) *hkl* indexing of the naturally grown facets.

mentioned here that, by adding saturated solution from time to time with gradual progress in the growth, the facets disappear and the crystal takes the exact same cylindrical shape along the length as that of the inner diameter of the SR ampoule. However, for the purpose of characterization along the desired directions and to prepare the crystal along the required direction for device fabrication, a few natural facets are very useful, as seen in Fig. 1(*c*).

2.2. Single-crystal and powder X-ray diffraction

The crystal structure of LAP was determined using the intensity data collected at room temperature (293 K) on a Nonius CAD-4 MACH3 diffractometer (graphite-monochromated Mo $K\alpha$, $\lambda = 0.71073$ Å). Powder X-ray diffraction analysis of the grown crystal was carried out using a PW1830 Philips Analytical powder X-ray diffractometer with Cu $K\alpha$ radiation (35 kV, 30 mA), scanning with a step size of 0.02° for the angular range 5–70° of 2θ, to determine the crystal system and lattice parameters.

2.3. Multicrystal X-ray diffractometry

To evaluate the crystalline perfection of the specimen crystals, HRXRD analysis was carried out. A multicrystal X-ray diffractometer, developed at the National Physical Laboratory (NPL), New Delhi (Lal & Bhagavannarayana, 1989), was used to record high-resolution rocking or diffraction curves (DCs). In this system, a fine-focus (0.4 × 8 mm; 2 kW Mo) X-ray source energized by a well stabilized Philips X-ray generator (PW1743) was employed. The well collimated and monochromated Mo $K\alpha_1$ beam obtained from three monochromator Si crystals set in the dispersive (+,−,−) configuration was used as the exploring X-ray beam. This arrangement improves the spectral purity ($\Delta\lambda/\lambda < 10^{-5}$) of the Mo $K\alpha_1$ beam. The divergence of the exploring beam in the horizontal plane (plane of diffraction) was estimated to be $<<3''$. The specimen crystal is aligned in the (+,−,−,+) configuration. Owing to the dispersive configuration of the third monochromator crystal with respect to the second monochromator, the spectral quality of the diffracted beam emerging from the third monochromator is highly perfect. Hence, though the lattice constant of the monochromator crystal and the specimen are different, the unwanted experimental dispersion broadening in the diffraction curve of the specimen crystal [$\Delta\text{FWHM} = \Delta\lambda/\lambda(\tan\theta_M - \tan\theta_S)$; θ_M and θ_S are the Bragg diffraction angles of the monochromator and the specimen crystals, respectively] is insignificant. The advantage of the dispersive configuration (+,−,−) over the nondispersive configuration (+,−,+) of monochromators is described by Bhagavannarayana & Kushwaha (2010). The specimen can be rotated about a vertical axis, which is perpendicular to the plane of diffraction, with a minimum angular interval of $0.4''$. The diffracted intensity is measured using a scintillation counter. The DCs were recorded by changing the glancing angle (angle between the incident X-ray beam and the surface of the specimen) around the Bragg diffraction peak position θ_B (taking zero as a reference point) starting from a suitable arbitrary glancing angle (θ). The detector was kept at the same angular position $2\theta_B$ with a wide opening for its slit, the so-called ω scan (Bhagavannarayana & Kushwaha, 2010). The ω scan is highly appropriate for recording the short-range-order scattering caused by defects, or the scattering from local Bragg diffraction from agglomerated point defects or due to low-angle and very low angle structural grain boundaries (Senthil Kumar *et al.*, 2011). Before the diffraction curve was recorded, the specimens were first lapped and chemically etched in a nonpreferential etchant of water and acetone mixed in a 1:2 volume ratio. This removes the noncrystallized solute atoms remaining on the surface of the crystal and also ensures the surface planarity.

2.4. TGA–DTA studies

Thermal analysis was used to find out the weight loss (thermogravimetric analysis, TGA) and energy change (differential thermal anaylsis, DTA) in the sample with respect to the temperature. The thermal analysis was carried out on the powder specimen of LAP by employing a Mettler Toledo Star simultaneous DTA/TGA analyser at a $10\ \text{K min}^{-1}$ heating rate in a nitrogen atmosphere using an alumina crucible.

2.5. Vickers micro-hardness studies

The hardness of a material is a measure of resistance offered by the lattice to permanent deformation. Vickers micro-indentation hardness studies were carried out using a hardness tester (OMNITECH; semi-automatic) equipped with a diamond pyramid indenter.

2.6. Dielectric studies

The dielectric properties of the grown single crystals were studied using an 'Alfa-A' high-frequency impedance analyser (Nova Control Technologies). Electrodes were made using electronic-grade silver paste on the parallel opposite surfaces of a rectangular specimen cut along ⟨100⟩ and ⟨010⟩ from the major surface to make firm electrical contacts. The frequency-dependent dielectric constant (ε_r) and dielectric loss ($\tan\delta$) of the crystal were measured at room temperature, in the frequency range of 10 Hz–5 MHz.

3. Results and discussion

3.1. Single-crystal and powder X-ray diffraction analysis

From the single-crystal XRD measurement it was confirmed that the grown crystal belongs to the monoclinic system having a noncentrosymmetric structure with space group $P2_1$. The cell parameters of LAP have been determined to be $a = 10.8576$, $b = 7.9171$, $c = 7.3192$ Å, and $\alpha = \gamma = 90°$, $\beta = 97.980°$. The observed values correspond well to the reported literature values (Herreros-Cedres *et al.*, 2003). The lattice parameters were refined with the *PowderX* refinement software (Dong, 1999) using the observed 2θ values as the input parameter. The refined values agree well with the single-crystal X-ray diffraction data. The indexed powder XRD pattern of the grown crystal is shown in Fig. 2.

3.2. High-resolution X-ray diffraction analysis

To analyse the crystalline perfection, high-resolution diffraction curves were recorded. The curve (*a*) in Fig. 3 shows the high-resolution DC recorded using (100) diffracting planes in symmetrical Bragg geometry by employing the multicrystal X-ray diffractometer with Mo $K\alpha_1$ radiation. As seen in the figure, the DC contains a single peak indicating that the specimen is free from structural grain boundaries. The FWHM of the DC is 12″, which is somewhat more than that expected from the plane-wave theory of dynamical X-ray diffraction (Batterman & Cole, 1964) but not far from the values that are generally observed for nearly perfect real-life bulk single crystals (Kumar *et al.*, 2011). The observed FWHM value indicates that the specimen crystal is not free from point defects and also one cannot rule out the presence of low-density dislocations. The strain field of the point defects and their aggregates is of spherical symmetry (Bhagavannarayana, Choubey *et al.*, 2005). However, the strain field of the dislocations is direction dependent. To gain a better understanding of the dislocations, two more DCs were recorded for the same specimen but for the different diffracting planes of (010) and (101) in symmetrical Bragg geometry under identical experimental conditions as that of curve (*a*); the DCs are given in (*b*) and (*c*), respectively, of Fig. 3. These curves are also single and sharp, confirming the absence of structural grain boundaries. The FWHM values of these curves are 10.5 and 12″, respectively. The direction of SR growth was along [010] and hence the diffraction vector **g** of the (010) planes is along the growth direction. The normals to the planes of (100) and (101) both lie in the same plane perpendicular to the growth direction and hence the **g** vector of these planes is perpendicular to the growth direction. Interestingly the FWHM of the (010) plane is lower (10.5″) than that of the (100) or (101) planes (which is 12″ for both). This indicates that the dislocations are of the edge type and parallel to the growth direction, *i.e.* along [100] as the strain field of the edge dislocations along the direction of the dislocation is at a minimum and maximum along the perpendicular direction. Etch pit studies on different faces using different solvents revealed the same type of orientation-dependent dislocations in LAP crystals (Sangwal *et al.*, 1995). The X-ray topographic technique is very sensitive and a direct method for such an observation; however, we could not get any such contrast in the intensity of topographs recorded for the same planes subjected to HRXRD owing to the low density of dislocations, as the minimum density required to achieve some contrast on the topographs is $\sim 10^5$ cm^{-2}. The present HRXRD analysis is nondestructive and better for assessing the overall crystalline perfection; moreover, it does not require any solvents as in the etching technique which may also introduce some artefacts and uncertainties. The present HRXRD studies reveal that the crystalline perfection is quite good with an important observation of the presence of low-density edge-type dislocations oriented along the growth direction.

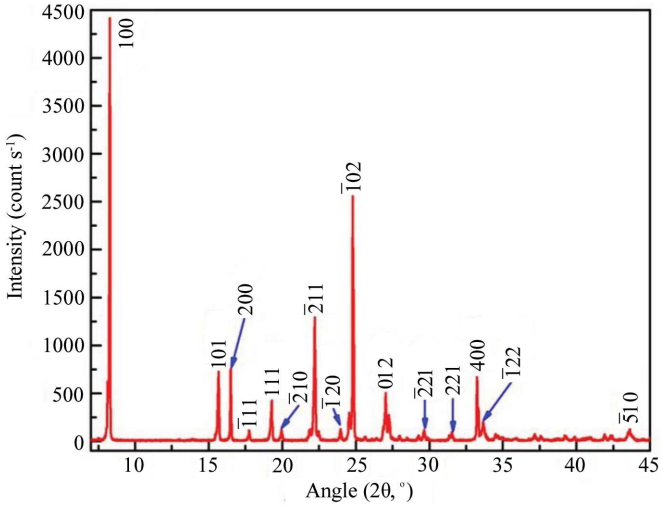

Figure 2
Powder X-ray diffraction pattern of the LAP single crystal.

3.3. Thermal analysis

The weight loss (TGA) and energy change (DTA) analyses of LAP samples were carried out in the temperature range

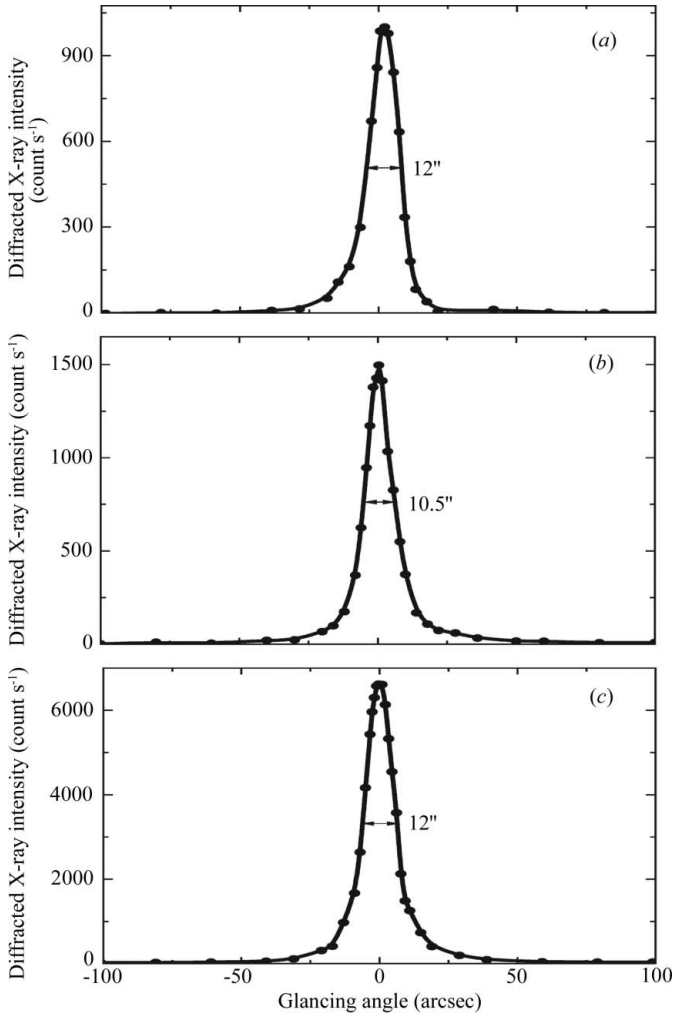

Figure 3
High-resolution diffraction curves recorded for LAP crystals: (*a*), (*b*) and (*c*) are, respectively, for (100), (010) and (101) diffracting planes.

303–1073 K in an alumina crucible in a nitrogen atmosphere; the TGA/DTA curves as a function of temperature are shown in Fig. 4. In the TGA spectrum no weight loss is observed in the temperature range below 383 K, showing the stability of the material below 383 K. The TGA graph shows no rapid loss of weight up to 463 K: around 1.5% between 388 and 423 K, and around 4% between 423 and 460 K. However, after this there is an enormous loss in weight, nearly 50%, from 463 to 760 K. The nature of this weight loss shows the decomposition of the material. In the DTA spectrum there is an endothermic peak at 397 K which reveals the melting point of the material, in good agreement with the present TGA result as well as the reported one (Mazumder *et al.*, 1995). The other endothermic peaks observed in the DTA curve, at 429, 521 and 596 K, are due to the decomposition of the volatile substances of carbon dioxide or ammonia, in good agreement with the TGA result. Other possible chemical reactions in this higher-temperature region are racemization and polymerization.

3.4. Mechanical analysis

Micro-hardness studies were conducted for loads ranging from 5 to 75 g with a constant indentation time of 10 s. The distance between any two consecutive indentations was kept more than five times the diagonal length of the indentation mark in order to avoid surface effects. Micro-hardness studies were carried out on two distinguished crystallographic faces, (100) and (010), to analyse the anisotropic nature of the grown crystal. At least five indentations were made on each face at each load. The average diagonal length of the indentation impression at each load was used for measuring the micro-hardness value (H_v).

Micro-hardness testing is one of the best methods to understand the mechanical properties of materials such as fracture behaviour, yield strength, brittle index and temperature of cracking (Lawn & Fuller, 1975; Westbrook, 1958). Good-quality crystals are needed for optical performance, especially second harmonic generation, with good mechanical behaviour. Micro-hardness values at each load for LAP crystals were calculated using the following expression:

$$H_v = 1.854\,P\,d^{-2}. \quad (1)$$

P is the load applied in kg and d the diagonal length in μm. The variation of hardness H_v with load P ranging from 5 to 75 g for planes (100) and (010) of the as-grown crystal is shown in Fig. 5(*a*). The difference obtained in H_v value for these planes clearly shows the anisotropic nature of the as-grown

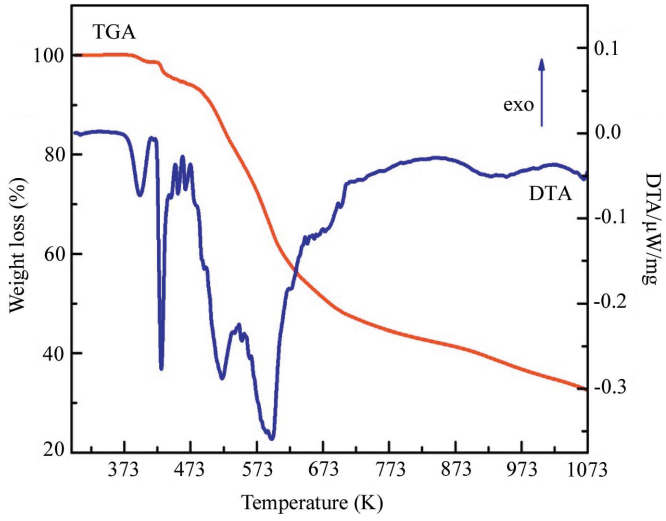

Figure 4
TG–DTA spectrum of the LAP single crystal.

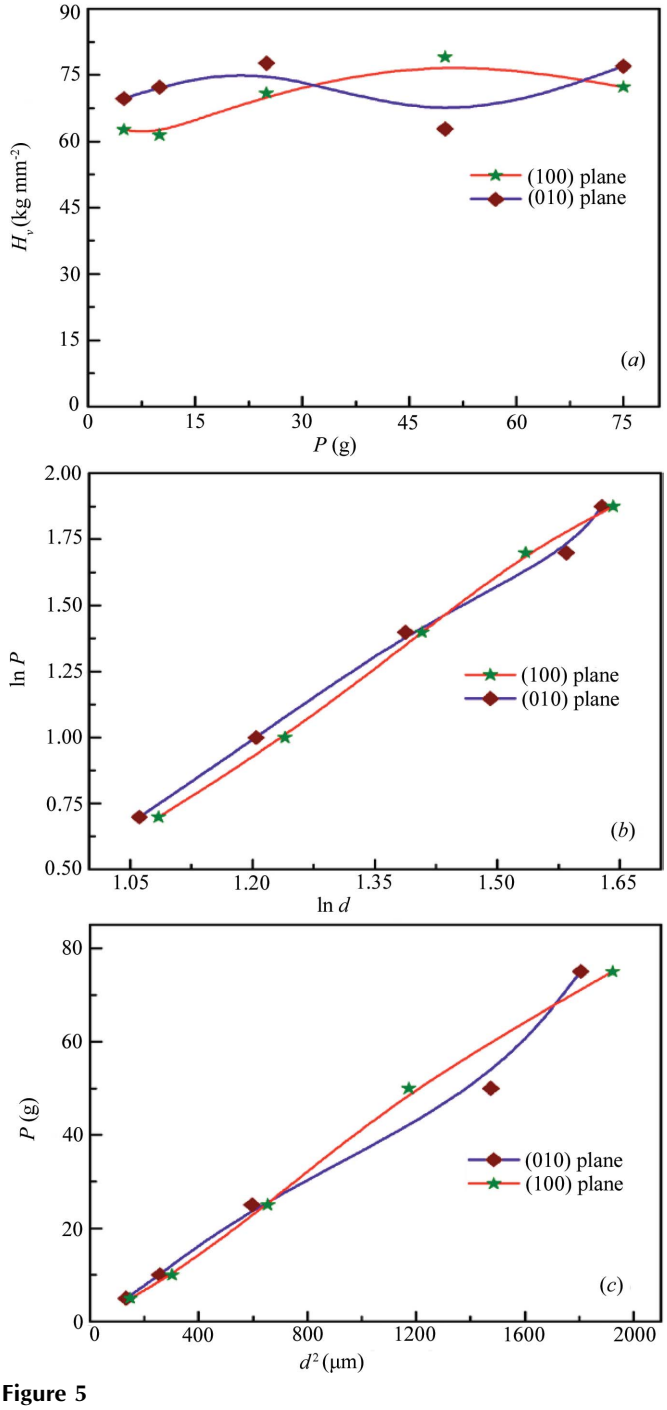

Figure 5
Micro-hardness testing along ⟨100⟩ and ⟨010⟩: (*a*) variation of Vickers hardness H_v with load P, (*b*) plots of ln$P$ *versus* ln$d$ and (*c*) plots of P *versus* d^2.

Table 1
Observed hardness parameters along the (100) and (010) planes of the LAP crystal.

	Meyer's law		Hays–Kendall approach		
Crystal	H_v (kg mm^{-2})	Meyers index (n)	W (g)	A_1	H_0 (kg mm^{-2})
LAP (100)	79.09	2.16	−2.394	0.041	76.014
LAP (010)	77.70	1.99	−0.033	0.038	71.749

sample. According to the normal indentation size effect (ISE), the micro-hardness of the crystal decreases with increasing load. The reverse is called the reverse indentation size effect (RISE), wherein the hardness increases with increasing load. From Fig. 5(*a*) it is evident that hardness increases with increasing load for the (100) plane after an initial fall and attains a maximum hardness value at 50 g. However, some dissimilarity is observed in H_v for the (010) plane: it has a higher hardness value at lower loads in comparison to the (100) plane, attains a maximum at 25 g and then falls, as shown in Fig. 5(*a*). With increasing load, the penetration depth increases and more dislocations are generated near the indentation site. A further increase of the load leads to the rearrangement of dislocations and the interaction of mutual stresses increases, resulting in a load-independent hardness value. The load variation can be interpreted using Meyer's law,

$$P = Ad^n, \tag{2}$$

where P is the applied load, d is the diagonal length of the impression, A is a constant and n is the Meyer's index (or the work-hardening coefficient). For normal ISE behaviour, the exponent n is less than 2. When $n > 2$, it is a reverse ISE behaviour, and when $n = 2$, hardness is independent of applied load (Kick's law). From the slope of the $\ln P$ *versus* $\ln d$ plot shown in Fig. 5(*b*), the estimated value of n is 2.16 for the (100) plane and 1.99 for the (010) plane. The difference obtained in the n value could be due to the anisotropic nature and orientation-dependent nature of the dislocations present in the crystal. According to Onitsch (1947) and Hanneman (1941), the value of n falls between 1 and 1.6 for hard materials and is more than 1.6 for soft ones. Thus the present crystal belongs to the soft material category, but it is found to be not as soft as other similar compounds (Priya *et al.*, 2008; Esthaku & Ramasamy, 2010; Dhanaraj & Rajesh, 2011). According to the Hays–Kendall approach (Hays & Kendall, 1973) load dependence of hardness is given by

$$P = W + A_1 d^2, \tag{3}$$

where W is the minimum load to initiate plastic deformation and A_1 is a load-independent constant. These two values have been estimated from the plot of P *versus* d^2 shown in Fig. 5(*c*), which is a straight line, where W is the intercept along the load axis and A_1 is the slope. The corrected hardness H_0 for these crystals has been estimated using the relation

$$H_0 = 1854\, A_1. \tag{4}$$

The hardness parameters for the (100) and (010) faces of the LAP crystal under study are given in Table 1.

3.5. Dielectric analysis

The dielectric properties are interconnected with the electro-optic properties of the crystals (Boomadevi & Dhanasekaran, 2004), particularly when they are non-conducting materials. An optical material with a high dielectric constant requires a larger poling voltage in order to polarize the dipoles and can suffer changes in the refractive index. Material that has an organic part normally has a low dielectric constant, eliminating the need for poling while maintaining the refractive index. The as-grown crystals were cut into rectangular pieces along the (100) and (010) planes and polished well before silver coating. The dielectric constant (ε_r) and loss ($\tan\delta$) of the LAP crystals were assessed to observe their variation due to the anisotropy with varying frequency at room temperature. The curves (*a*) and (*b*) in Fig. 6 depict ε_r and $\tan\delta$, respectively, as a function of frequency. It is clear from plot (*a*) that the room-temperature values of ε_r gradually decrease as the frequency increases. All of the four polarizations dipolar, ionic, space charge and electronic contribute in the low-frequency region (Rajanrajan *et al.*, 2007) in both planes. The low dielectric constant of the crystal at high frequency is attributed to space-charge polarization (Rao & Smakula, 1965). This is the normal dielectric behaviour in the high-frequency region and may be a result of negligible space-charge and dipolar polarization in this range, where only ionic and electronic parts are active (Kushwaha *et al.*, 2008). The ε_r value obtained for the (100) plane is ∼10.5

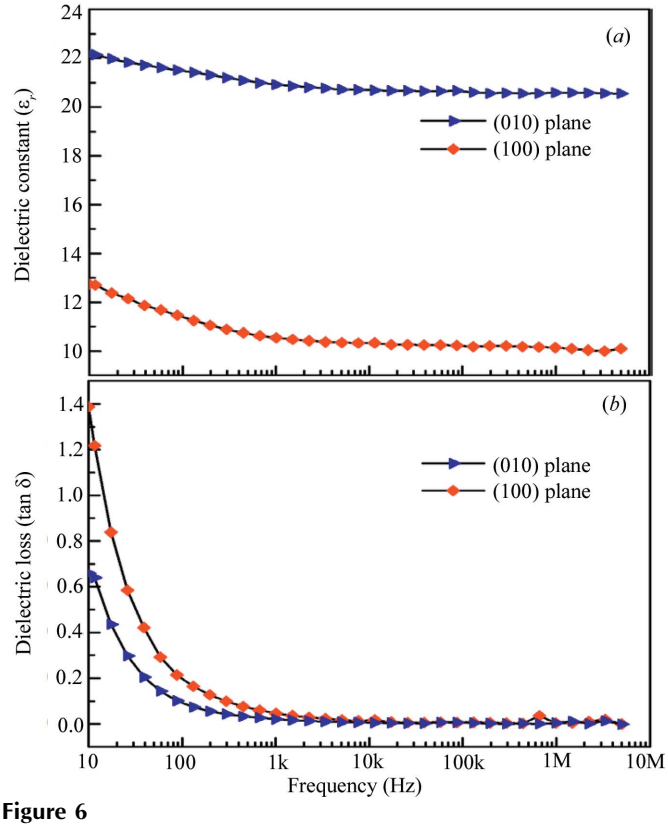

Figure 6
The relative dielectric constant (*a*) and loss (*b*) of the LAP single crystal in the frequency range 10 Hz–5 MHz.

and for the (010) plane is ~21. The difference obtained in ε_r with the orientation is due to the anisotropic nature of the material (Shakir *et al.*, 2010; Bando *et al.*, 2011). The $\tan\delta$ plot (Fig. 6*b*) indicates that the loss factor decreases with frequency. The characteristic of low dielectric constant and dielectric loss at higher frequencies for a given sample suggests that the sample possesses enhanced optical quality with fewer defects, and this parameter is of vital importance for various NLO materials and their applications (Balarew & Dushlew, 1984). The $\tan\delta$ values for both planes are very small and quite similar in the higher-frequency region. However, in the lower-frequency region a clear difference is visible, revealing the anisotropic nature of the material. The dielectric properties showing the low density of defects are in tune with the HRXRD studies.

4. Conclusions

A good-quality large single crystal of the title compound was successfully grown for the first time by the unidirectional SR method and the grown crystal was subjected to different characterization analyses. The structure of the material was confirmed by single-crystal and powder XRD methods and its lattice dimensions were determined. The crystalline perfection of the grown single crystals was studied by HRXRD and the results revealed that the grown crystal has good crystalline perfection without having any structural grain boundaries. The high-resolution diffraction curves reveal the presence of a very low density of edge dislocations along the growth direction. It is observed from the micro-hardness studies that the LAP crystal belongs to the soft material category but is harder than many semi-organic compounds. The observed stable dielectric constant and low loss values indicate that the grown bulk crystal was free from major defects, in tune with the HRXRD results. The present studies of crystalline perfection of the LAP single crystal along with the mechanical and dielectric properties, the bulk growth ability with the proposed SR method, the reconfirmed SHG efficiency (which is three times that of KDP), and the optical and thermal stability reveal that the LAP crystal is suitable for electro-optic modulator applications for the entire characterized frequency range 10 Hz–5 MHz.

The authors acknowledge Professor R. C. Budhani, Director, NPL, for his constant encouragement for crystal growth activity at NPL. BR acknowledges the University Grant Commission for providing a research fellowship.

References

Anandan, P., Saravanan, T., Parthipan, G., Mohan Kumar, R., Bhagavannarayana, G., Ravi, G. & Jayavel, R. (2011). *Solid State Sci.* **13**, 915–922.

Angeli, M. P. A. & Dhanuskodi, S. (2001). *Spectrochim. Acta A*, **57**, 2345–2353.

Arjunan, S., Bhaskaran, A., Mohan Kumar, R., Mohan, R. & Jayavel, R. (2010). *J. Alloys Compd.* **506**, 784–787.

Badan, J., Hierle, R., Perigaud, A., Zyss, J. & Williams, D. J. (1993). Editors. *NLO Properties of Organic Molecules and Polymeric Materials*, American Chemical Symposium Series, Vol. 233. Washington, DC: American Chemical Society.

Balamurugan, S. & Ramasamy, P. (2009). *Spectrochim. Acta A*, **71**, 1979–1983.

Balarew, C. & Dushlew, R. (1984). *J. Solid State Chem.* **55**, 1–6.

Bando, K., Kumeta, S., Sasaki, F. & Hotta, S. (2011). *Jpn. J. Appl. Phys.* **50**, 101603.

Baruch, A., Fuchs, B. A., Syn, C. K. & Velsko, S. P. (1989). *Appl. Opt.* **28**, 4465–4472.

Batterman, B. W. & Cole, H. (1964). *Rev. Mod. Phys.* **36**, 681–717.

Bhagavannarayana, G., Ananthamurthy, R. V., Budakoti, G. C., Kumar, B. & Bartwal, K. S. (2005). *J. Appl. Cryst.* **38**, 768–771.

Bhagavannarayana, G., Budakoti, G. C., Maurya, K. K. & Kumar, B. (2005). *J. Cryst. Growth*, **282**, 394–401.

Bhagavannarayana, G., Choubey, A., Shubin, Yu. V. & Lal, K. (2005). *J. Appl. Cryst.* **38**, 448–454.

Bhagavannarayana, G., Kumar, S., Shakir, M., Kushawaha, S. K., Maurya, K. K., Malhotra, R. & Rao, K. R. (2010). *J. Appl. Cryst.* **43**, 710–715.

Bhagavannarayana, G. & Kushwaha, S. K. (2010). *J. Appl. Cryst.* **43**, 154–162.

Bhagavannarayana, G., Rajesh, P. & Ramasamy, P. (2010). *J. Appl. Cryst.* **43**, 1372–1376.

Boomadevi, S. & Dhanasekaran, R. (2004). *J. Cryst. Growth*, **261**, 70–76.

Dong, C. (1999). *J. Appl. Cryst.* **32**, 838.

Dhanaraj, G., Srinivasan, M. R. & Bhat, H. L. (1991). *J. Raman Spectrosc.* **22**, 177–181.

Dhanaraj, P. V. & Rajesh, N. P. (2011). *Phys. B*, **406**, 12–18.

Esthaku, P. M. & Ramasamy, P. (2010). *Mater. Lett.* **64**, 1–3.

Hameed, H. A. S. & Rohani, S. (2007). *Mater. Lett.* **61**, 5141–5144.

Hanneman, M. (1941). *Metall. Manchu.* **23**, 135–140.

Hays, C. & Kendall, E. G. (1973). *Metallography*, **6**, 275–282.

Herreros-Cedres, J., Hernandez-Rodriguez, C., Gonzalez-Diaz, B. & Guerrero-Lemus, R. (2003). *Appl. Phys. B*, **77**, 607–612.

Kim, Y. K. & Lal, R. B. (1998). *J. Mater. Sci. Lett.* **17**, 1363–1365.

Kushwaha, S. K., Vijayan, N. & Bhagavannarayana, G. (2008). *Mater. Lett.* **62**, 3931–3933.

Lal, K. & Bhagavannarayana, G. (1989). *J. Appl. Cryst.* **22**, 209–215.

Lawn, B. R. & Fuller, E. R. (1975). *J. Mater. Sci.* **9**, 2016–2024.

Mazumder, A., Kar, T., Prasad, S. & Gupta, S. (1995). *Jpn. J. Appl. Phys.* **34**, 5717–5720.

Misoguti, L., Varela, A. T., Nunes, F. D., Bagnato, V. S., Melo, F. E. A., Mendes Filho, J. & Zilio, S. C. (1996). *Opt. Mater.* **6**, 147–152.

Monaco, S. B., Davis, L. E., Velsko, S. P., Wang, F. T. & Eimerl, D. (1987). *J. Cryst. Growth*, **85**, 252–255.

Onitsch, E. M. (1947). *Mikroskopia*, **2**, 131–135.

Priya, M. N. S., Varghese, B., Linet, M. J., Bhagavannarayana, G., Raj, J. C., Krishnan, S., Dinakaran, S. & Das, J. S. (2008). *Cryst. Growth Des.* **8**, 1663–1667.

Rajanrajan, K., Mani, G., Vetha Potheher, I., Jesudurai, J. G. M., Vimalan, M., Christy, D., Madhavan, J. & Sagayaraj, P. (2007). *J. Phys. Chem. Solids*, **68**, 2370–2375.

Rao, K. V. & Smakula, A. (1965). *J. Appl. Phys.* **36**, 2031–2038.

Sangwal, K., Servat, J., Sanz, F. & Torrent-Burgues, J. (1997). *J. Cryst. Growth*, **180**, 263–273.

Sangwal, K., Torrent-Burgues, J., Sanz, F. & Servat, J. (1997). *J. Cryst. Growth*, **180**, 274–279.

Sangwal, K., Veintemillas-Verdaguer, S. & Torrent-Burgues, J. (1995). *J. Cryst. Growth*, **154**, 364–369.

Sankaranarayanan, K. & Ramasamy, P. (2005). *J. Cryst. Growth*, **280**, 467–473.

Senthil Kumar, K., Moorthy Babu, S. & Bhagavannarayana, G. (2011). *J. Appl. Cryst.* **44**, 313–318.

Senthil Pandian, M., Balamurugan, N., Bhagavannarayana, G. & Ramasamy, P. (2008). *J. Cryst. Growth*, **310**, 4143–4147.

Shakir, M., Riscob, B., Maurya, K. K., Ganesh, V., Wahab, M. A. & Bhagavannarayana, G. (2010). *J. Cryst. Growth*, **312**, 3171–3177.

Westbrook, J. H. (1958). Report 58-RL-2033. General Electric Research Laboratory, USA.

Zaitseva, N. & Carman, L. (2001). *Prog. Cryst. Growth Charact.* **43**, 1–118.